RSC Advances

PAPER

View Article Online
View Journal | View Issue

Cite this: *RSC Adv.*, 2023, **13**, 18864

Stability and structure–activity relationship of the SPA4 peptide under ambient and stressed conditions of lung injury

Asif Alam Chowdhury, [a] Karla Rodgers, [b] Nachiket M. Godbole [a] and Shanjana Awasthi *[a]

Lung inflammation and injuries are major health problems. The SPA4 peptide (amino acid sequence GDFRYSDGTPVNYTNWYRGE) binds to Toll-like receptor-4 and exerts anti-inflammatory activity. In this study, we have determined the stability of the structure and structure–activity relationship of the SPA4 peptide under ambient and stressed conditions of lung injury. The SPA4 peptide was maintained at different pH and temperatures, in solutions of different ionic strengths, and simulated lung fluids. The primary and secondary structure of the SPA4 peptide was determined by ultraviolet-visible (UV-VIS) and circular dichroism (CD) spectroscopy. The activity of the SPA4 peptide was determined by measurement of secreted levels of chemokine C–X–C motif ligand 1/keratinocyte-derived chemokine (CXCL1/KC) and lactate by primary mouse lung epithelial cells against lipopolysaccharide (LPS) stimuli. Our results demonstrate the stability of the structure of the SPA4 peptide at room temperature and 4 °C over 10 days. The original UV-VIS spectra of the SPA4 peptide followed a typical pattern when incubated in solutions of pH 5.7, 7.0, and 8.0 at different temperatures, simulated lung fluids, and most of the chemical components. Slight shifts in the absorbance peaks, derivative values, and vibrational fine structures were noted in the fourth-derivative spectra of the SPA4 peptide under some conditions. An increased level of lactate is the hallmark of lung injury. The SPA4 peptide on its own and in the presence of lactate exerts anti-inflammatory activity. The primary and secondary structure and the activity of the SPA4 peptide remain intact when pre-incubated in 2 mM sodium lactate solution. The results provide important insights about the stability and structure–activity relationship of the SPA4 peptide.

Received 2nd May 2023
Accepted 12th June 2023

DOI: 10.1039/d3ra02918b

rsc.li/rsc-advances

Introduction

Toll-like receptor 4 (TLR4) is a transmembrane receptor that recognizes specific pathogen-and damage-associated molecular patterns. One of the major ligands of TLR4 is Gram-negative bacterial lipopolysaccharide (LPS). The LPS-induced activation of TLR4 results in acute inflammation, tissue damage, and injury.[1] The SPA4 peptide (amino acid sequence GDFRYSDGTPVNYTNWYRGE) was identified from a TLR4 interacting region of surfactant protein-A (SP-A), which binds to the activated TLR4 and reduces inflammation.[2,3] Intratracheal administration of the SPA4 peptide suppresses inflammation and injury and improves the pulmonary function parameters and survival in mouse models of lung infection and inflammation.[3–5]

Although therapeutic administration of SPA4 peptide has been effective in lung inflammation models, it is likely to get exposed to varying stressed conditions in respiratory tract. The lung microenvironment undergoes significant changes during inflammation. One of the hallmarks is the change in pH of lung microenvironment. The luminal side of the airway epithelia is lined by a thin layer of fluid called airway surface liquid.[6] The airway surface liquid is derived mainly from submucosal gland secretions and transepithelial hydro-osmotic movements. The airway surface liquid pH in normal respiratory tract ranges between 5.6 and 6.7 in the nasal mucosa, around 7.0 in bronchia, 7.1 in lower airways and 6.6 in upper airways (reviewed in ref. 7 and 8). Historically, acidification of the airway surfaces has been suggested as a measure of airway disease,[6] specifically during cystic fibrosis[9,10] and asthma.[11] The pH of bronchoalveolar fluid was noted as 6.21 and 6.89 in patients with stable and acute exacerbation chronic obstructive pulmonary diseases, respectively.[12] Acidic pH is promoted by lung inflammation due to production of metabolic acids by recruited leukocytes[8,13] as well as an increased secretion of acid by airway epithelial cells through activation of apical H^+ channels.[14]

[a]*Department of Pharmaceutical Sciences, University of Oklahoma Health Sciences Center, 1110 N. Stonewall Avenue, Oklahoma City, OK-73117, USA. E-mail: Shanjana-Awasthi@ouhsc.edu; Fax: +1-405-271-7505; Tel: +1-405-271-6593 extn 47332*

[b]*Department of Microbiology and Immunology, University of Oklahoma Health Sciences Center, 940 Stanton L. Young Blvd, Oklahoma City, OK-73104, USA*

The extracellular acidosis can further activate neutrophils, delay apoptosis, and enhance an inflammatory response.[15]

In addition to altered pH, significant changes have been observed in biochemical composition or metabolome of lung microenvironment during injury. The changes in amino acid and lipid metabolic pathways, deranged energy metabolism, and disturbed cellular turnover are noted.[16–20] The simulated fluids with varying pH and biochemical composition have been used to mimic the lung microenvironment under healthy and diseased states. Two of the most common simulated lung fluids are Gamble's solution and artificial lysosomal fluid (ALF). Gamble's solution represents the healthy condition of the lung lining fluid with neutral pH 7.4, and ALF has been used to replicate the lysosomal compartment simulating phagolysosome with acidic pH 4.5 (as reviewed in[21]). Among several biochemical entities, an increased lactate production in lung is associated with severity of lung injury.[22–25] An elevated blood lactate concentration (>2 mmol L^{-1}) is significantly associated with morbidity and 30 day mortality of the patients with acute respiratory distress syndrome.[26] Among Gamble's solution and ALF, the lactate is present only in ALF.[21]

The objective of the current study was to assess the stability of the structure of SPA4 peptide under ambient conditions at different pH and temperatures and in simulated lung fluids and in presence of chemical components representing normal and inflammatory lung microenvironment. The anti-inflammatory activity of SPA4 peptide was studied in primary mouse lung epithelial cell system against LPS stimuli. Our results demonstrate an intact structure of the SPA4 peptide under ambient conditions. The primary structure of SPA4 peptide is not affected by pH 5.7–8.0 or temperatures 25–37 °C. The original UV-VIS spectral pattern remains unaltered when SPA4 peptide is incubated in Gamble's solution, ALF, and most of the individual chemical components except for sodium hydroxide solution at prescribed concentration. However, changes in peaks, derivative values, and vibrational fine structures were noted in fourth derivative spectra of SPA4 peptide in some conditions. The SPA4 peptide treatment exerts anti-inflammatory response in primary mouse lung epithelial cell system against LPS stimuli. Furthermore, our results demonstrate maintenance of the primary and secondary structure and anti-inflammatory activity of the SPA4 peptide when incubated in 2 mM sodium lactate solution. These results provide important insights about the stability and structure–activity relation of SPA4 peptide under ambient condition and in the presence of chemical components altered during lung injury.

Materials and methods

SPA4 peptide

The SPA4 peptide (amino acid sequence GDFRYSDGTPV-NYTNWYRGE) was synthesized at Genscript, NJ. Mass spectroscopy and high-performance liquid chromatography (HPLC) confirmed the composition and purity, respectively. All the batches of SPA4 peptide were ≥95% HPLC-pure. The stock solution of SPA4 peptide (834.2 μM) was maintained in endotoxin-free water at −20 °C. Endotoxin-free water was used for preparation of different solutions and as a vehicle. We have used term water throughout for endotoxin-free water.

Mice

Male C57BL6 mice (5–6 weeks old) were purchased from the Jackson laboratory (Bar Harbor, ME). The mice were housed for at least 1 week for acclimatization before the start of experiments. Up to five mice were housed together. All experiments with mice were performed in compliance with the Public Health Service Policy on Humane Care and Use of Laboratory Animals. The animal studies were approved by the Institutional Animal Care and Use Committee (Protocol number: 20-054-SCHIR) at the University of Oklahoma Health Sciences Center (OUHSC).

Ultraviolet-visible (UV-VIS) spectroscopy

The UV-VIS spectroscopy was used to determine any changes in primary structure of the SPA4 peptide as described earlier.[5,27] Briefly, an aliquot of 2 μl was loaded onto a well of microvolume glass slide plate (Take3 plate, Agilent, Santa Clara, CA). The UV-VIS absorbance readings or optical density (OD) values were recorded at 200–750 nm wavelengths with an interval of 5 nm and optical pathlength of 0.5 mm. The buffer solutions containing an equivalent volume of vehicle served as blank. The blank-subtracted OD readings were plotted.

Fourth-order derivative spectra (second derivative of second derivative) of original UV-VIS spectra were obtained and analyzed for area under the curve (AUC), number of peaks above the baseline, and vibrational fine structures related to phenylalanine (F), tyrosine (Y) and tryptophan (W) residues of SPA4 peptide under different conditions using GraphPad Prism software, which utilizes the Savitzky and Golay's principle of differentiation of data.[28,29]

Primary structure or stability of the SPA4 peptide over time and at different pH and temperatures. The stock solution of SPA4 peptide (834.2 μM) was kept at room temperature or at 4 °C for a period of 10 days, and an aliquot was subjected to UV-VIS spectroscopy at an interval of 24 h as described above.

In another set of experiments, the SPA4 peptide was diluted to 100 μM in citrate buffer (pH 3.0), phosphate buffer solutions with the pH of 5.7, 7.0 and 8.0, and *N*-cyclohexyl-2-aminoethanesulfonic acid or CHES solution (pH 10.0; Table 1). The buffer solutions were prepared according to previously published reports.[30–32] Prepared solutions of SPA4 peptide in phosphate buffered solutions of different pH were kept in a preheated water bath at 25 °C, 30 °C, 32 °C, and 37 °C for 1 h. After 1 h of incubation, the aliquots of SPA4 peptide solutions were subjected to UV-VIS spectroscopy as described above. The water alone or water diluted in respective solutions served as blank.

Structure of the SPA4 peptide in simulated lung fluid solutions and in the presence of individual chemical components. To evaluate SPA4 peptide stability in simulated lung fluids, the stock solution of SPA4 peptide (834.2 μM) was diluted to 100 μM in Gamble's solution (pH 7.4) and artificial lysosomal

Table 1 Concentrations of chemical ingredients of citrate buffer (pH 3.0), phosphate buffer (pH 5.7, 7.0, and 8.0), and *N*-cyclohexyl-2-aminoethanesulfonic acid (CHES, pH 10.0) solution

Ingredients (stock concentration)	pH 3.0	pH 5.7	pH 7.0	pH 8.0	pH 10.0
Monobasic sodium phosphate (0.2 M)		0.0935 M	0.039 M	0.0053 M	
Dibasic sodium phosphate (0.2 M)		0.0065 M	0.061 M	0.0947 M	
Citric acid (0.1 M)	0.093 M				
Sodium citrate (0.1 M)	0.007 M				
CHES					0.5 M
SPA4 peptide (834.2 μM)	100 μM	100 μM	100 μM	100 μM	100 μM

Table 2 Composition of simulated lung fluid solutions (Gamble's solution and ALF). All solutions were prepared in endotoxin-free water

Components	Manufacturer	Gamble's solution (pH 7.4)	ALF (pH 4.5)
Calcium chloride	Sigma, St. Louis, MO	2.5 mM (0.277 g L^{-1})	0.87 mM (0.097 g L^{-1})
Magnesium chloride	Sigma, St. Louis, MO	1 mM (0.095 g L^{-1})	0.52 mM (0.050 g L^{-1})
Sodium chloride	VWR-BDH, West Chester, PA	103 mM (6.019 g L^{-1})	54.93 mM (3.21 g L^{-1})
Sodium citrate dihydrate	Fisher Scientific, Hampton, NH	0.33 mM (0.097 g L^{-1})	0.262 mM (0.077 g L^{-1})
Sodium phosphate dibasic	US biological, Swampscott, MA	1 mM (0.142 g L^{-1})	0.5 mM (0.071 g L^{-1})
Sodium sulfate	Sigma, St. Louis, MO	0.5 mM (0.071 g L^{-1})	0.275 mM (0.039 g L^{-1})
Potassium chloride	Sigma, St. Louis, MO	4 mM (0.298 g L^{-1})	
Sodium acetate trihydrate	Fisher Scientific, Fairlawn, NJ	7 mM (0.953 g L^{-1})	
Sodium bicarbonate	VWR chemicals, Solon, OH	31 mM (2.604 g L^{-1})	
Citric acid	Ward's Science, St. Catherines, ON, Canada		108.26 mM (20.8 g L^{-1})
Glycine	Sigma, St. Louis, MO		0.785 mM (0.059 g L^{-1})
Sodium hydroxide	Ameresco life Science, Solon, OH		150 mM (6.0 g L^{-1})
Sodium lactate	Sigma, St. Louis, MO		0.758 mM (0.085 g L^{-1})
Sodium pyruvate	Sigma, St. Louis, MO		0.781 mM (0.086 g L^{-1})
Sodium tartrate dihydrate	EMS, Hatfield, PA		0.391 mM (0.090 g L^{-1})

fluid (ALF, pH 4.5). The composition of Gamble's solution and ALF is described in Table 2. The solutions containing SPA4 peptide were kept at room temperature for 24 h. The UV-VIS absorbance readings then were taken as described above. Similarly, UV-VIS spectroscopy was performed for SPA4 peptide (100 μM) in presence of each of the components of Gamble's solution and ALF. Higher concentrations (0.5 M and 1 M) of each component were also included, except sodium phosphate dibasic and sodium bicarbonate solutions. An equivalent volume of water instead of peptide was added to simulated lung fluids or chemical solutions which served as blank for spectroscopic analysis.

Circular dichroism (CD) spectroscopy

The SPA4 peptide (417 μM) was incubated in 2 mM sodium lactate solution at room temperature for 24 h. The SPA4 peptide then was diluted to 83.4 μM concentration in methanol while maintaining 2 mM concentration of sodium lactate. The spectra were recorded on a Jasco J-715 CD spectropolarimeter with a PTC-348 WI Peltier temperature controller as described earlier.[33,34] The samples for CD spectroscopy were maintained at a temperature of 20 °C, and spectra were obtained using a 0.1 cm cuvette pathlength with three accumulations per spectrum. The CD spectra of samples containing SPA4 peptide were corrected by subtracting spectra of solvent mix containing equivalent volume of water in place of the peptide.

SPA4 peptide activity

We determined the SPA4 peptide activity in primary mouse lung epithelial cell system.

Isolation of mouse lung epithelial cells. Primary lung epithelial cells were isolated from mice using a combination of previously published methods.[35,36] The age-matched mice were anesthetized by isoflurane and euthanized by cervical dislocation. The diaphragm was cut to expose the heart and the lung. The inferior vena cava was cut, and ice-cold Dulbecco's phosphate buffered saline (DPBS) was injected into the right ventricle to drain out the blood. About 0.5 ml of 50 U ml^{-1} dispase II solution (Roche, Basel, Switzerland) was injected into the lung through the trachea. The lungs then were incubated in dispase II solution on a shaker-incubator for 1 h at 25 °C. The dispase-digested lungs were transferred in McCoy's 5A medium (Life Technologies, Carlsbad, CA) containing 5% fetal bovine serum (FBS) and 50 μg ml^{-1} gentamicin (Quality Biological, Gaithersburg, MD), and mechanically minced. Minced lung suspension was filtered through 70 μm and 20 μm sterile filter strainers and centrifuged at 300×*g* for 10 min at room temperature.

Next, the lung epithelial cells were separated from single lung cell suspension using Optiprep™ (60% Iodixanol, Serum Bernburg AG, Bernburg, Germany) density gradient technique developed by Viscardi *et al.*[36] Briefly, a solution of 1.08 g ml^{-1} Optiprep density was overlayered with an equivalent volume of 1.04 g ml^{-1} Optiprep density solution. The lung cell suspension then was layered on top of the gradient and centrifuged at 400×*g* for 20 min

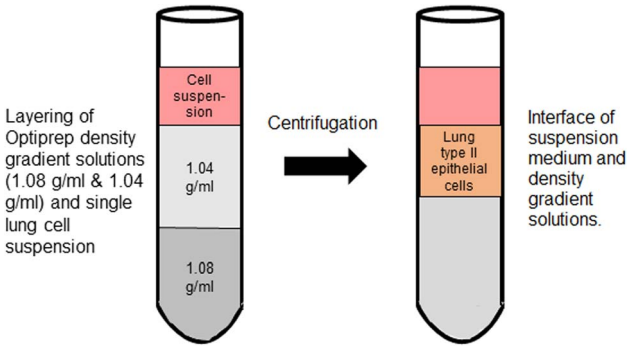

Fig. 1 Separation of primary mouse lung epithelial cells by density gradient centrifugation. Lung cell suspension was layered on top of the Optiprep density gradient solutions of 1.04 and 1.08 g ml^{-1} and centrifuged. The layering and separation of lung epithelial cells are depicted within the figure.

at room temperature (Fig. 1). Isolated lung epithelial cells were collected from the band at around 1.056 g ml^{-1} just below the interface of cell suspension and gradient. Collected cells were centrifuged and washed at 490×*g* for 5 min at room temperature. The cell pellet was resuspended in McCoy's 5A medium containing 5% FBS and 50 μg ml^{-1} gentamicin and subjected to serum panning. Sterile Petri dishes were coated with 1 : 200 diluted serum overnight at 4 °C. The cell suspension was layered on the serum-coated plate and incubated for 1 h at room temperature. Finally, nonadherent lung epithelial cells were collected and centrifuged at 770×*g* for 5 min at room temperature.

Expression of pro-surfactant protein-C (SP-C), a marker of type II lung epithelial cells. Isolated cells were suspended in McCoy's 5A medium containing 5% FBS and 50 μg ml^{-1} gentamicin and seeded in 8 well-chamber slides at the density of 250 000 cells per well and incubated overnight. The cells were washed and fixed with 4% paraformaldehyde and permeabilized with 0.1% triton-X 100 (Thermo Fisher Scientific, Waltham, MA). Nonspecific sites were blocked by incubating the cells with 1% bovine serum albumin (BSA) solution for 1 h. The cells then were stained with 1 : 500 diluted rabbit anti-pro-SP-C antibody (Sigma, St. Louis, MO) overnight at 4 °C, washed, and incubated in 1 : 200 diluted Alexa Fluor 568-conjugated goat anti-rabbit IgG antibody (Abcam, Waltham, MA) for 1 h at room temperature. After washing with DPBS, the cells were stained with 1 : 2000 diluted Hoechst 33342 dye (nuclear stain, Thermo Fisher Scientific, Waltham, MA). The immunostained cells were mounted using ProLong Gold anti-fade reagent (Thermo Fisher Scientific, Waltham, MA). The imaging was done by Leica SP8 confocal microscope at 40× objective. Photomicrographs were taken from random regions.

LPS challenge and treatment with SPA4 peptide. Isolated primary lung epithelial cells were seeded at the density of 300 000–600 000 cells per well in 24-well plates and cultured in McCoy's 5A medium containing 5% FBS and 50 μg ml^{-1} gentamicin. After overnight incubation, the cells were washed and challenged with 1 μg ml^{-1} purified *Pseudomonas aeruginosa* 10-derived LPS (Sigma, St. Louis, MO) and treated with 100 μM SPA4 peptide (freshly thawed or pre-incubated in water, 2 mM sodium lactate [higher concentration than 0.758 mM in simulated lung fluid ALF, Table 2] or 500 mM sodium lactate for 24 h) after 1 h of LPS challenge.

The cell-free supernatants were harvested after 24 h of LPS challenge. Briefly, the cell culture medium was collected and centrifuged at 170×*g* at 4 °C. The cell free-supernatants were collected and stored at −80 °C.

Secreted levels of lactate

The secreted levels of lactate were measured in cell-free supernatants using a commercially available lactate assay kit (Biovision, Waltham, MA) per manufacturer's instructions. Briefly, the cell-free supernatants were diluted 1 : 50 in the lactate assay buffer provided with the kit and centrifuged at 14 000×*g* for 20 min in 10 kDa spin columns (Abcam, Waltham, MA) to remove lactate dehydrogenase. Fifty μl of reaction mix containing 46 μl lactate assay buffer, 2 μl lactate enzyme mix and 2 μl lactate probe was added to 50 μl of filtered supernatants and incubated for 30 min under dark at room temperature. Absorbance was then measured at 570 nm wavelength in a microplate reader (Agilent, Santa Clara, CA). Amounts of lactate were normalized per number of cells and compared with those detected in unchallenged, vehicle-treated cells.

Determination of CXCL1/KC in cell-free supernatants

A commercially available ELISA kit was used to measure the levels of CXCL1/KC in cell-free supernatants (R&D systems, Minneapolis, MN) per manufacturer's instructions. Briefly, the wells of 96-well of Immulon® 4 HBX high protein binding affinity ELISA strips (Thermo Fisher Scientific, Waltham, MA) were coated with 2 μg ml^{-1} rat anti-mouse CXCL1/KC capture antibody overnight at room temperature. The wells then were washed, and non-specific binding sites were blocked with 1% BSA solution in DPBS. The antibody-coated wells were incubated with diluted recombinant mouse CXCL1/KC standard solutions and 1 : 5 or 1 : 10 diluted cell-free supernatants overnight at 4 °C. After washing, the wells were incubated with 50 ng ml^{-1} biotinylated rat anti-mouse CXCL1/KC detection antibody for 2 h followed by 1 : 40 diluted streptavidin-horse radish peroxidase solution for 20 min at room temperature. The immune complexes were detected by adding tetramethylbenzidine substrate solution (Sigma, St. Louis, MO). The reaction was stopped by adding 2 N H_2SO_4, and optical density (OD) was read spectrophotometrically at 450 nm and 540 nm. The OD values at 540 nm were subtracted from their respective OD values at 450 nm wavelength to adjust for any optical imperfections of the plates per the manufacturer's instructions. The unchallenged, vehicle-treated cells served as control. The measured amounts of CXCL1/KC were normalized per number of cells and compared with those detected in cell-free supernatants from unchallenged, vehicle-treated cells or LPS-challenged, vehicle-treated cells.

Statistical analysis

Data were analyzed using *t*-test or ANOVA (GraphPad Prism, San Diego, CA), and $p < 0.05$ was considered statistically significant or otherwise indicated.

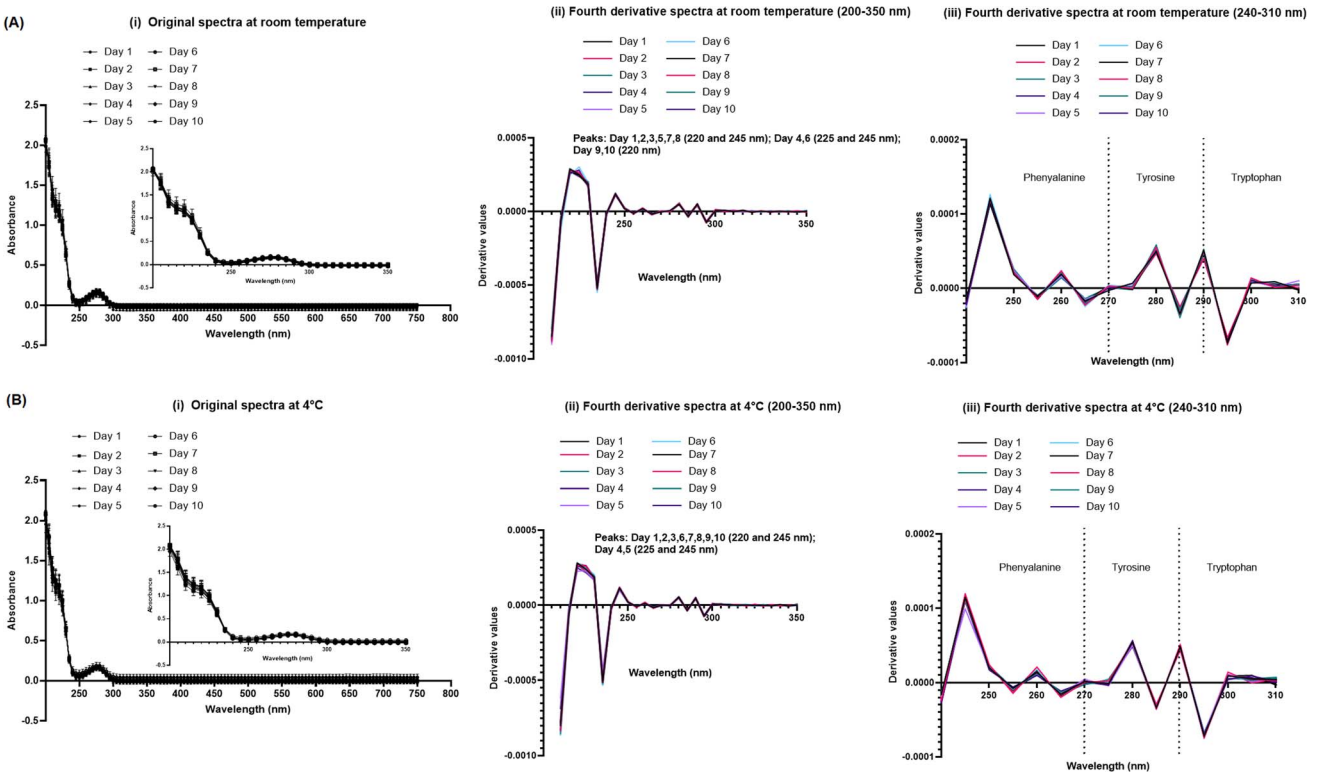

Fig. 2 The stock solution of the SPA4 peptide in endotoxin-free water (834.2 μM) was incubated at room temperature or at 4 °C for a period of 10 days, and absorbance readings were taken against water as blank. The results are blank subtracted absorbance readings (mean ± SEM) at 5 nm interval between the range of 200–750 nm wavelength (i). The fourth-derivative spectra of original UV-VIS spectra with all blank subtracted absorbance values were obtained using Graphpad Prism for peak identification between the wavelength range of 200–350 nm. Peaks are indicated within the figure (ii). The fourth-derivative results were plotted for derivative values in the range of 240–310 nm wavelength (iii). Absorbance peaks at specific wavelengths are identified within the figure. Results are derived from triplicate runs in three separate experiments performed on different occasions.

Results

Primary structure of SPA4 peptide in ambient conditions (4 °C and room temperature) over time

Original and fourth-derivative UV-VIS spectra overlapped for 834.2 μM SPA4 peptide (stock solution) kept at room temperature or at 4 °C over a period of 10 days (Fig. 2). Only the blank subtracted absorbance readings were considered for plotting the UV-VIS spectra. The fourth-derivative spectra were analyzed for identification of peaks or any shift in peaks of aromatic amino acids. The SPA4 peptide encodes one phenylalanine, three tyrosine, and one tryptophan residues. Although peaks of these aromatic amino acids may overlap, we divided the fourth-derivative spectra (240–310 nm) into three regions for (240–270 nm) phenylalanine, (270–290 nm) tyrosine, and (290–310 nm) tryptophan amino acids for analyzing any changes in the peaks or vibrational fine structures.[29]

UV-VIS spectra of the SPA4 peptide at different pH (range 3.0–10.0) and temperatures (range 25–37 °C)

The UV-VIS spectroscopy (200–750 nm) then was performed for the 100 μM SPA4 peptide incubated for 1 h at 25 °C, 30 °C, 32 °C, and 37 °C in phosphate buffer solutions (pH 5.7, 7.0, and 8.0), citrate buffer (pH 3.0), and CHES solution (pH 10.0, Table 1). The 100 μM concentration of SPA4 peptide was used in activity assays and in our previously published report.[5] The original UV-VIS spectra showed typical primary structure of SPA4 peptide at pH 5.7, 7.0, and 8.0 (Fig. 3) as described previously.[5,27] Lower absorbance readings were noted between 200–250 nm wavelengths for the SPA4 peptide maintained in respective buffer solutions at pH 3.0 and 10.0. Similarly, the shifts in peaks were noted in the fourth-derivative spectra. The shifts in the peaks or changes in derivative values were prominent for phenylalanine residue of SPA4 peptide at pH of 3.0. Similarly, an increased derivative value was obtained at 260 nm for SPA4 peptide at pH 10.0 when incubated at 37 °C (Fig. 3).

Primary structure of the SPA4 peptide in simulated lung fluids and in presence of the chemical components at different concentrations

The SPA4 peptide was diluted to 100 μM final concentration in Gamble's solution (pH 7.4) and ALF (pH 4.5, Table 2) and incubated at room temperature for 24 h. No changes were observed in original UV-VIS spectra of SPA4 peptide in these solutions (Fig. 4A). However, when fourth derivatives of original spectra were analyzed, the peaks differed for the SPA4 peptide

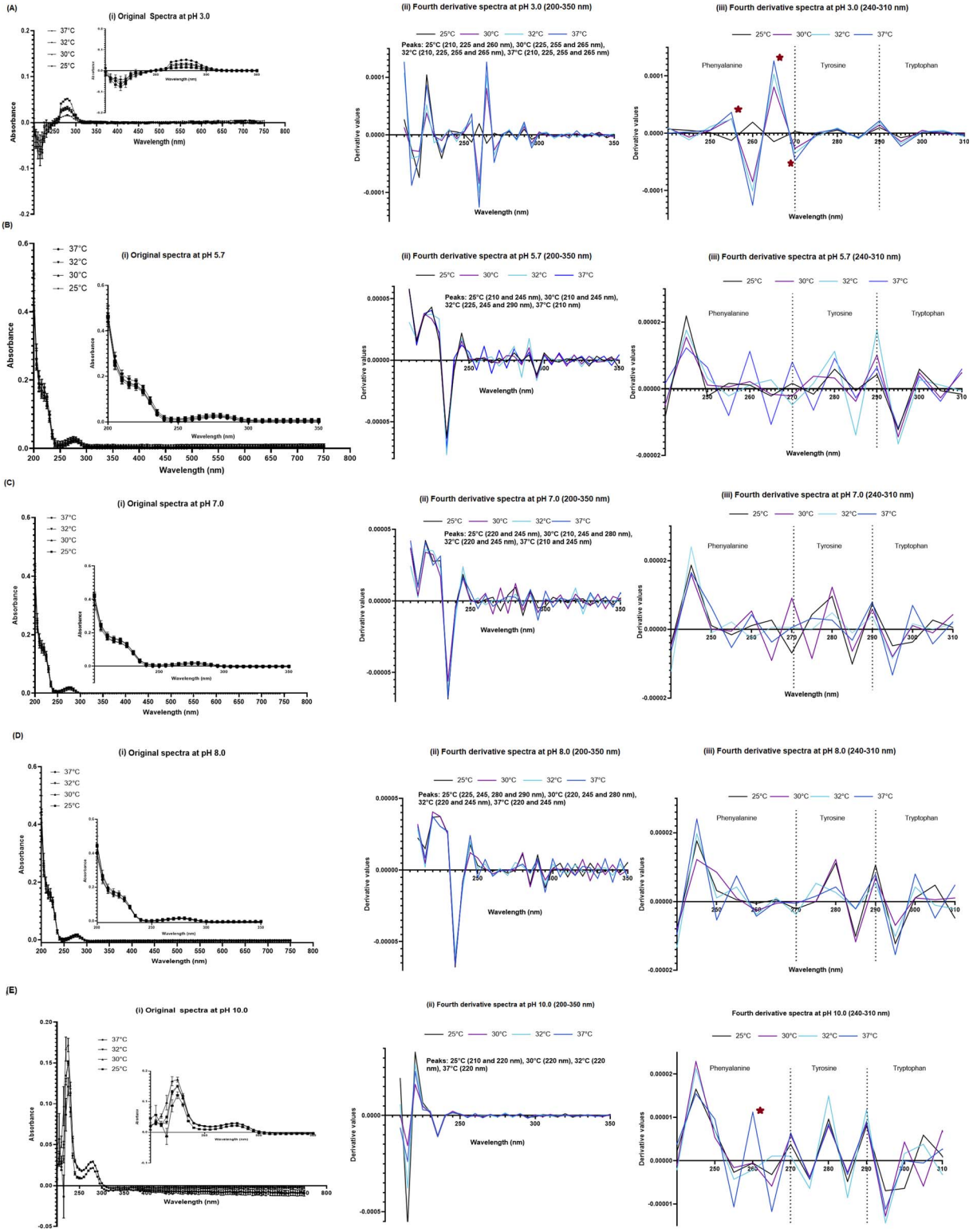

Fig. 3 UV-VIS spectra of 100 μM SPA4 peptide at different pH and temperatures. Absorbance reading were gathered for SPA4 peptide solutions in citrate buffer (pH 3.0, (A)), phosphate buffer solutions (pH 5.7, 7.0, and 8.0, (B–D)), and CHES buffer (pH 10.0, (E)) at temperatures 25 °C, 30 °C, 32 °C, & 37 °C. The composition of respective buffers is provided in Table 1. The SPA4 peptide suspended in water was included in each run. An equivalent volume of water suspended in respective buffers was maintained in prescribed conditions and served as blank. The UV-VIS spectra of blank subtracted absorbance readings (mean ± SEM) (i), fourth derivative of original UV-VIS spectra (ii), and derivative values in the range of 240–310 nm wavelength (iii) are shown. Absorbance peaks at specific wavelengths are identified within the figure. Any shift in the peaks, change in derivative values, and vibrational fine structures for aromatic amino acids of the SPA4 peptide are indicated with an asterisk. Results are derived from triplicate runs in three separate experiments performed on different occasions.

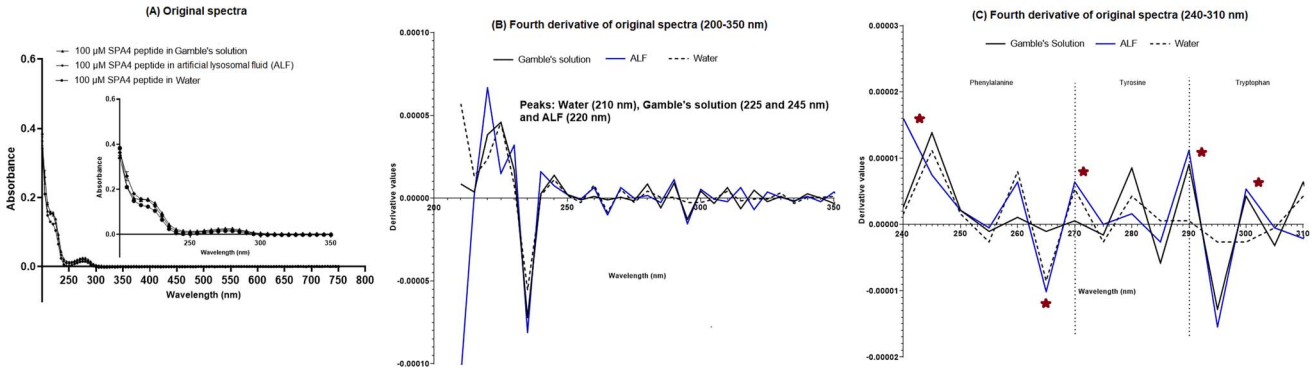

Fig. 4 UV-VIS spectroscopy of 100 μM SPA4 peptide suspended in simulated lung fluids (Gamble's solution and ALF). The SPA4 peptide was incubated in respective solutions for 24 h at room temperature before UV-VIS spectroscopy. The SPA4 peptide suspended in water was included in each run. An equivalent volume of water was maintained in respective buffers in prescribed condition and served as blank. Original UV-VIS spectra are shown for the blank subtracted absorbance readings at the interval of 5 nm in the range of 200–750 nm wavelengths. The results are shown as mean ± SEM (A). Fourth-derivative readings in the range of 200–350 nm (B) and 240–310 nm (C) wavelengths were analyzed. Absorbance peaks at specific wavelengths are identified within the figure. Any shift in the peaks, change in derivative values, and vibrational fine structures for aromatic amino acids of the SPA4 peptide are indicated with an asterisk. Results are derived from triplicate runs in three separate experiments performed on different occasions.

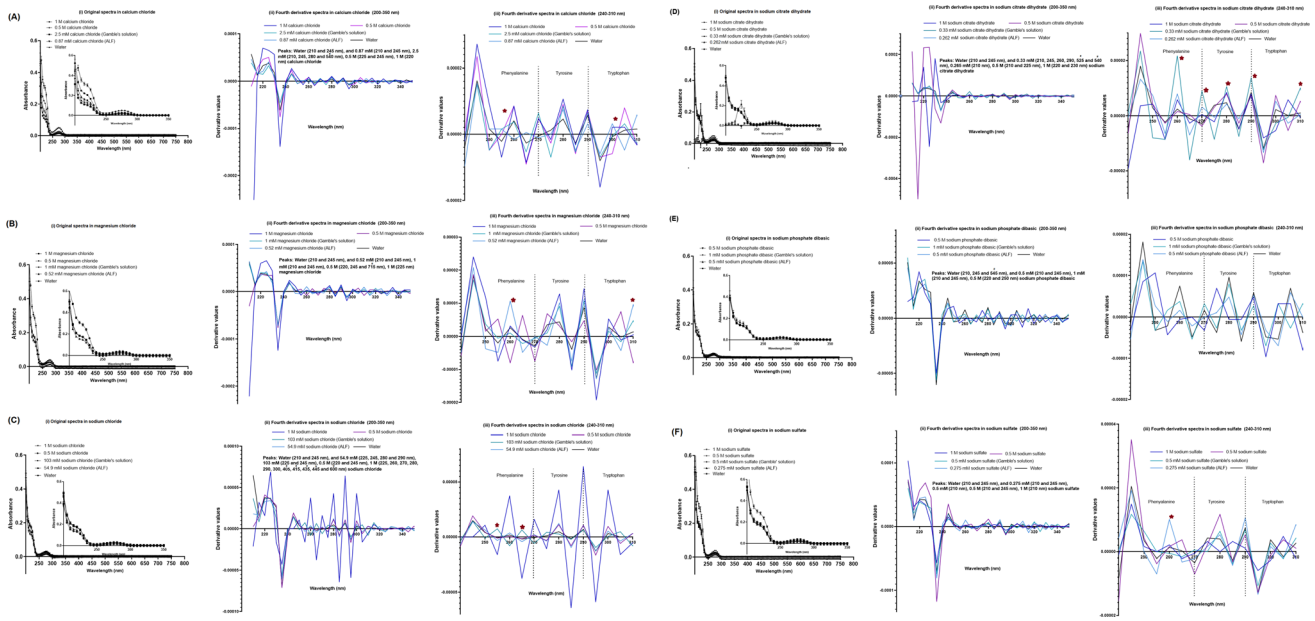

Fig. 5 UV-VIS spectra of the SPA4 peptide (100 μM) suspended in individual chemical components common in both simulated lung fluids (Gamble's solution and ALF) at prescribed concentrations per Table 2 (also identified within the figure) and at higher concentrations (0.5 M and 1 M). The SPA4 peptide suspension was prepared in respective chemical solutions: calcium chloride (0.87 mM, 2.5 mM, 0.5 M, and 1 M, (A)), magnesium chloride (0.52 mM, 1 mM, 0.5 M, and 1 M, (B)), sodium chloride (54.9 mM, 103 mM, 0.5 M, and 1 M, (C)), sodium citrate dihydrate (0.262 mM, 0.33 mM, 0.5 M, and 1 M, (D)), sodium phosphate dibasic (0.5 mM, 1 mM, and 0.5 M, (E)), and sodium sulfate (0.275 mM, 0.5 mM, 0.5 M, and 1 M, (F)). The original UV-VIS spectra (200–750 nm, mean ± SEM of absorbance readings, (i)) and fourth-derivative spectra (200–350 nm and 240–310 nm, (ii, iii)) of blank subtracted absorbance readings are included. Absorbance peaks at specific wavelengths are identified within the figure. Additional peaks beyond 350 nm wavelength are identified as # symbol. Any shift in the peaks, change in derivative values, and vibrational fine structures for aromatic amino acids of the SPA4 peptide are indicated with an asterisk. An equivalent volume of water was maintained in respective chemical solutions under prescribed condition and served as blank. Results are derived from triplicate runs in three separate experiments performed on different occasions.

in simulated lung fluids (225 and 245 nm in Gamble's solution, 220 nm in ALF, Fig. 4B). The peaks at different wavelengths indicate the vibrational shift of phenylalanine residue when diluted in Gamble's solution and ALF. A slight shift towards lower wavelength was also observed in the tryptophan region (Fig. 4C).

We also evaluated the effect of individual chemical ingredients of simulated lung fluids on UV-VIS spectra of the SPA4

peptide. The SPA4 peptide diluted in water and in individual chemicals solutions at higher concentrations (0.5 M and 1 M) served as controls. The peptide was replaced with an equivalent amount of water in blank solutions. The results are presented for the UV-VIS spectra of SPA4 peptide (100 μM) in ingredients common in Gamble's solution and ALF (Fig. 5) or are part of Gamble's solution (Fig. 6) or ALF (Fig. 7). There was no significant change in the original UV-VIS spectral pattern or absorbance values of the SPA4 peptide maintained in simulated lung fluids and components, except in the sodium hydroxide solution. Also, slightly lower absorbance values were noted for SPA4 peptide maintained in magnesium chloride, sodium lactate, sodium pyruvate, and sodium tartrate dihydrate solutions at prescribed concentrations. Shifts in peaks, positive or negative direction of peaks, and derivative values were noted for the SPA4 peptide when diluted in Gamble's solution, ALF, and some of the individual components (Fig. 5–7).

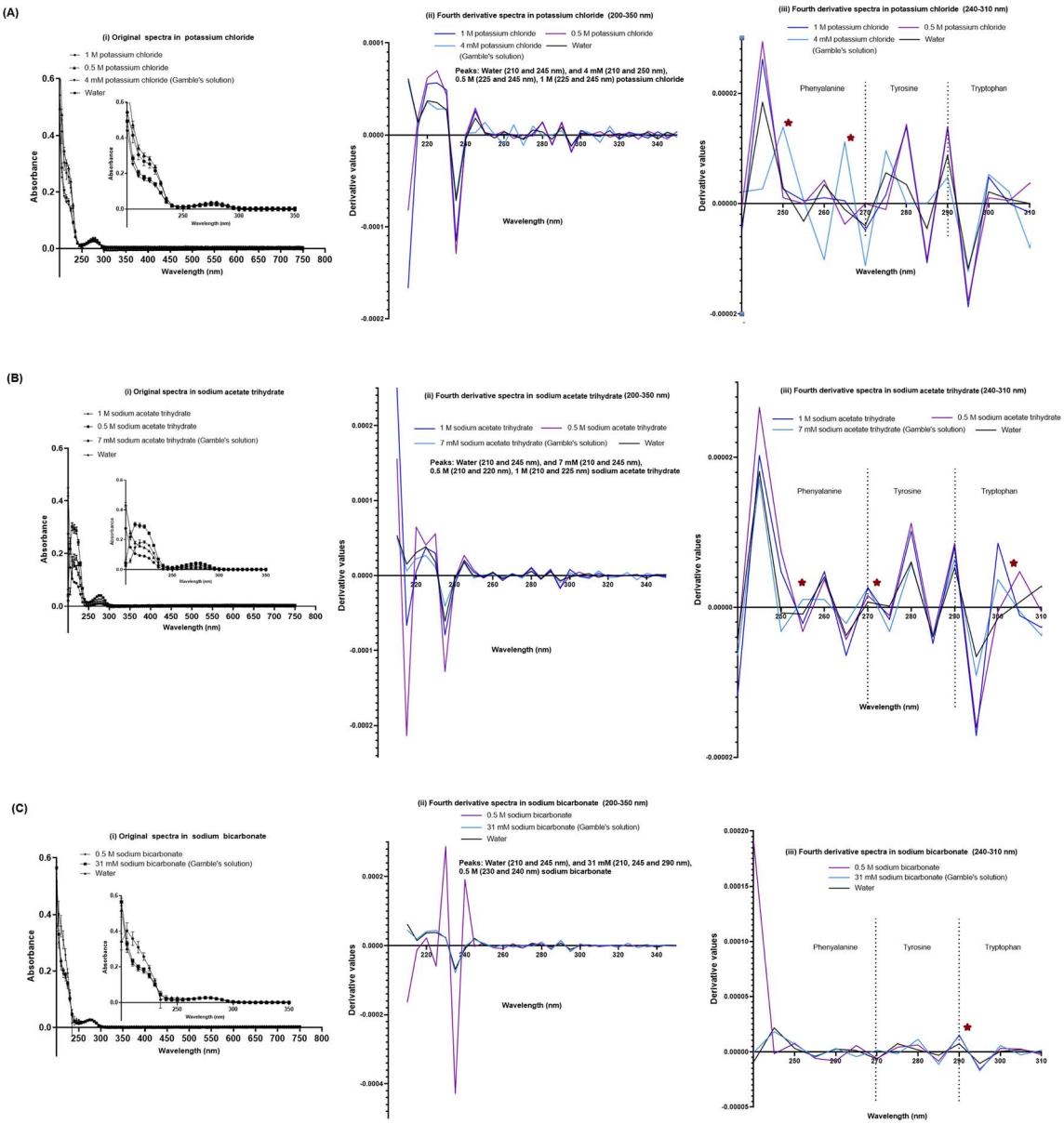

Fig. 6 UV-VIS spectra of the SPA4 peptide (100 μM) suspended in individual chemical components specific to Gamble's solution in addition to those included in Fig. 5 at prescribed concentrations per Table 2 and at higher concentrations (0.5 M and 1 M). The SPA4 peptide suspension was prepared in respective chemical solutions of potassium chloride (4 mM, 0.5 M, and 1 M, (A)), sodium acetate trihydrate (7 mM, 0.5 M, and 1 M, (B)), and sodium bicarbonate (31 mM and 0.5 M, (C)). The original UV-VIS spectra (200–750 nm, mean ± SEM of absorbance readings, (i)) and fourth-derivative spectra (200–350 nm and 240–310 nm, (ii, iii)) of blank subtracted absorbance readings are included. An equivalent volume of water was maintained in respective chemical solutions under prescribed condition and served as blank. Absorbance peaks at specific wavelengths are identified within the figure. Any shift in the peaks, change in derivative values, and vibrational fine structures for aromatic amino acids of the SPA4 peptide are indicated with an asterisk. Results are derived from triplicate runs in three separate experiments performed on different occasions.

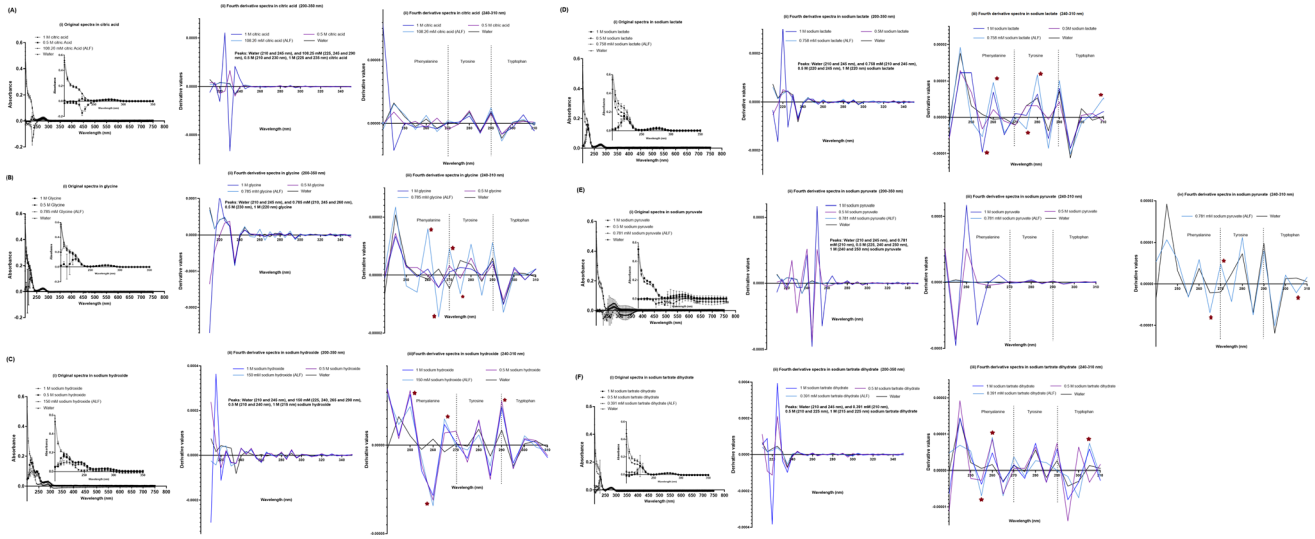

Fig. 7 UV-VIS spectra of the SPA4 peptide (100 μM) suspended in individual chemical components specific to ALF in addition to those included in Fig. 5 at prescribed concentrations per Table 2 and at higher concentrations (0.5 M and 1 M). The SPA4 peptide suspension was prepared in respective chemical solutions of citric acid (108.26 mM, 0.5 M, and 1 M, (A)), glycine (0.785 mM, 0.5 M, and 1 M, (B)), sodium hydroxide (150 mM, 0.5 M, and 1 M, (C)), sodium lactate (0.758 mM, 0.5 M, and 1 M, (D)), sodium pyruvate (0.781 mM, 0.5 M, and 1 M, (E)), and sodium tartrate dihydrate (0.391 mM, 0.5 M, and 1 M, (F)). The original UV-VIS spectra (200–750 nm, mean ± SEM of absorbance readings, (i) and fourth-derivative spectra (200–350 nm and 240–310 nm, (ii, iii) of blank subtracted absorbance readings are included. An equivalent volume of water was maintained in respective chemical solutions under prescribed condition and served as blank. Absorbance peaks at specific wavelengths are identified within the figure. Any shift in the peaks, change in derivative values, and vibrational fine structures for aromatic amino acids of the SPA4 peptide are indicated with an asterisk. Results are derived from triplicate runs in three separate experiments performed on different occasions.

SPA4 peptide treatment reduces the secreted levels of CXCL1/KC and lactate in primary mouse lung epithelial cells against *P. aeruginosa* LPS

To determine the activity of the SPA4 peptide, we isolated primary mouse lung epithelial cells. Ninety eight percent of the primary mouse lung epithelial cells were viable. The isolated cells were uniform in morphology and stained for pro-SP-C, a precursor protein of SP-C and a marker of lung type II epithelial cells (Fig. 8).

As expected, the *P. aeruginosa* LPS challenge stimulated the secretion of CXCL1/KC (895.4 pg ml^{-1}) and lactate (39.5 nmol) per 100 000 primary mouse lung epithelial cells over a period of 24 h. However, the SPA4 peptide treatment reduced the secreted levels of LPS-stimulated CXCL1/KC (502.4 pg ml^{-1}, $p < 0.05$ *versus* LPS-challenged, vehicle-treated cells) and lactate (35 nmol, $p = 0.09$ *versus* LPS-challenged, vehicle-treated cells). The amounts of CXCL1/KC and lactate in the SPA4 peptide treatment group were not statistically different from those in the unchallenged, vehicle-treatment group (Fig. 9).

Primary and secondary structure of SPA4 peptide in 2 mM sodium lactate solution

The primary structure of SPA4 peptide (417 μM) was maintained when incubated in 2 mM sodium lactate solution (higher concentration than 0.758 mM in simulated lung fluid ALF, Table 2) for 24 h at room temperature compared to that in water (Fig. 10A). Original UV-VIS and fourth-derivative spectra overlapped for SPA4 peptide in 2 mM sodium lactate and water. Furthermore, the CD spectroscopy demonstrated intact secondary structure of SPA4 peptide (83.4 μM, Fig. 10C) compared to that in water as published earlier.[5,27,33] However, low absorbance readings between 200–220 nm wavelengths suggest an effect on peptide backbone of SPA4 peptide in the presence of 500 mM sodium lactate (Fig. 10B).

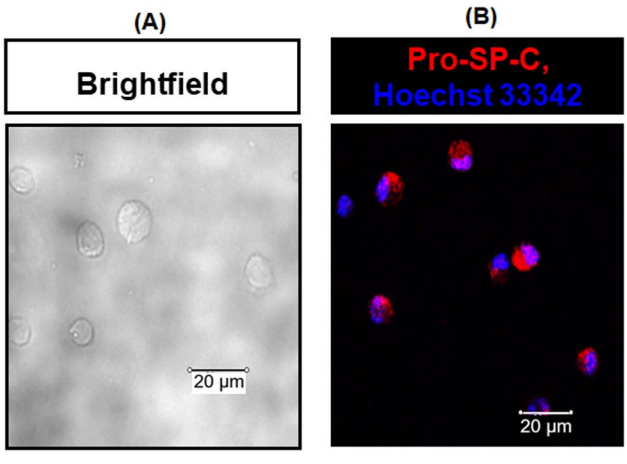

Fig. 8 Isolated primary mouse lung epithelial cells were uniform in morphology and expressed pro-SP-C protein (marker of type II lung epithelial cells). Representative brightfield photomicrographs of isolated cells are shown in (A). The harvested cells stained for pro-SP-C (in red) and cell nuclei (in blue) were analyzed by confocal microscopy. Representative confocal photomicrographs of stained cells are included in (B). The photomicrographs are representative of two experiments.

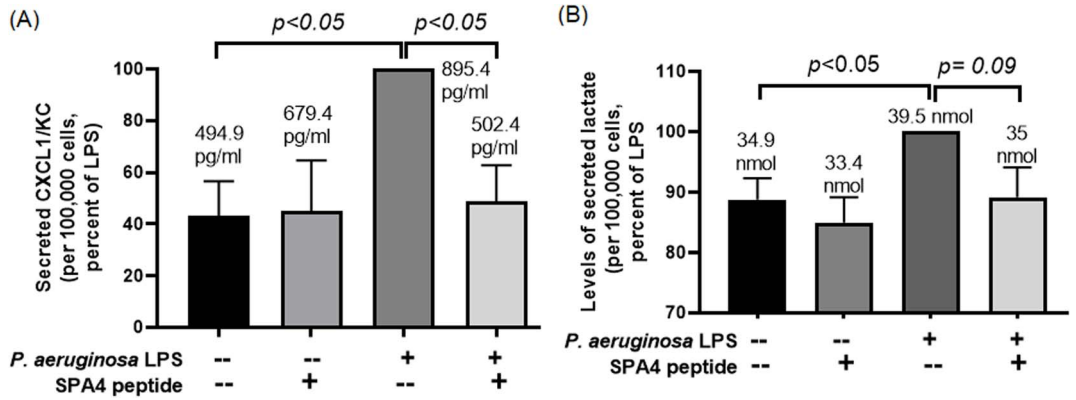

Fig. 9 SPA4 peptide treatment suppresses the LPS-induced secretion of CXCL1/KC (A) and lactate (B) in primary mouse lung epithelial cells. The cells were challenged by 1 μg ml^{-1} *P. aeruginosa* LPS and treated with 100 μM SPA4 peptide. The cell-free supernatants were collected after 24 h of LPS challenge, and levels of CXCL1/KC and lactate were measured by using an ELISA or biochemical assay, respectively. Measured levels of analytes were normalized with 100 000 cells. The bars show (mean + SEM) normalized values as percentage of those for LPS-challenged cells. Average values are indicated within the figure. Results are derived from three separate experiments performed on separate occasions. Statistical significance was determined by *t*-test.

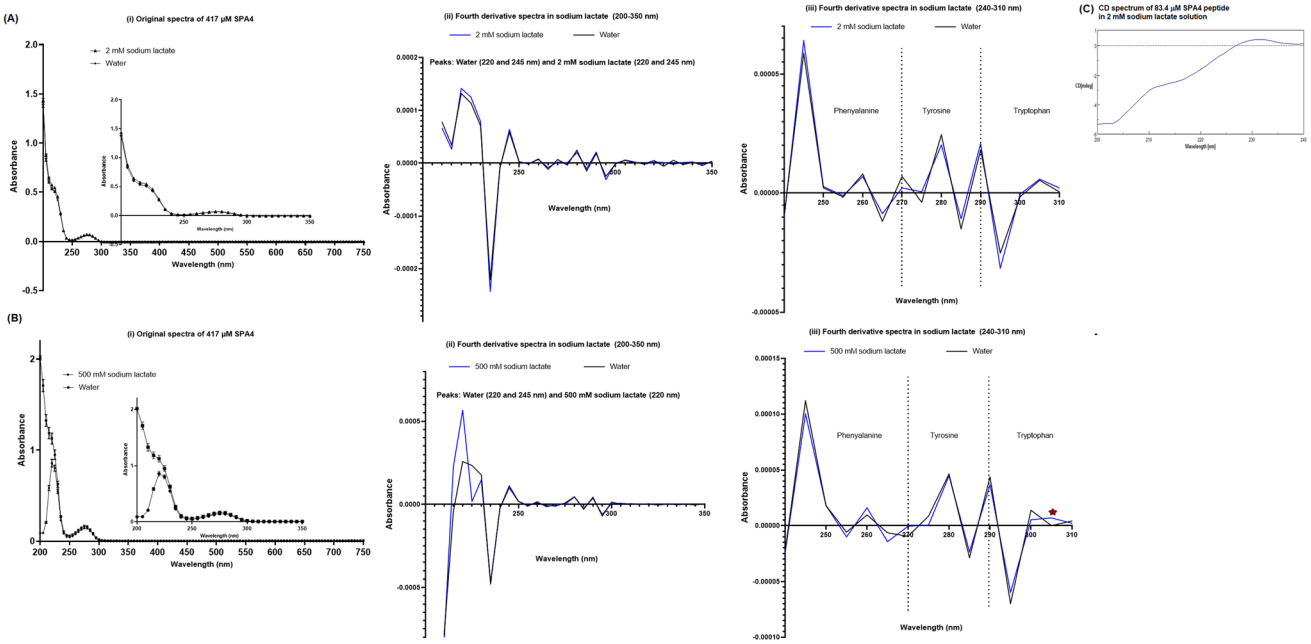

Fig. 10 Structure of the SPA4 peptide after pre-incubation in 2 mM sodium lactate (A, C) and 500 mM sodium lactate (B) solutions for 24 h at room temperature. The original UV-VIS spectra (200–750 nm, mean ± SEM of absorbance readings, (A and B (i))) and fourth-derivative spectra (200–350 nm and 240–310 nm, A and B (ii, iii)) of blank subtracted absorbance readings of SPA4 peptide (417 μM) are included. An equivalent volume of water was maintained in respective chemical solutions under prescribed condition and served as blank. Absorbance peaks at specific wavelengths are identified within the figure. Results are derived from triplicate runs in three separate experiments performed on different occasions. Representative CD spectrum of the SPA4 peptide (83.4 μM) pre-incubated in 2 mM sodium lactate solution for 24 h at room temperature is shown in (C).

Structure–activity relation of SPA4 peptide

We further examined the activity of SPA4 peptide (at 417 μM concentration) pre-incubated in sodium lactate solutions or water at room temperature for 24 h and diluted to 100 μM for treatment of primary mouse lung epithelial cells. Consistently, the SPA4 peptide with intact structure in 2 mM sodium lactate solution or in vehicle significantly suppressed the LPS-induced secretion of CXCL1/KC (Fig. 11). However, SPA4 peptide with its disrupted structure in 500 mM sodium lactate solution did not affect the LPS-induced CXCL1/KC secretion.

Discussion

The activity of a peptide can be affected by several factors including pH, ionic strength, and chemicals and metabolites

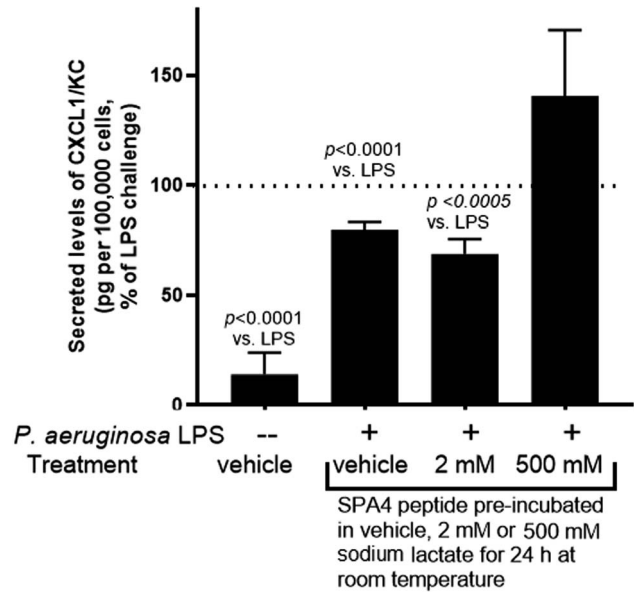

Fig. 11 Intact structure of SPA4 peptide after incubation in 2 mM sodium lactate solution maintains the anti-inflammatory activity against LPS stimuli. The SPA4 peptide (417 μM) was pre-incubated in water (vehicle), 2 mM sodium lactate, or 500 mM sodium lactate solutions for 24 h. Primary mouse lung epithelial cells then were challenged with *P. aeruginosa* LPS (1 μg ml^{-1}) and treated with 100 μM SPA4 peptide after 1 h of LPS challenge. Secreted levels of CXCL1/KC were measured in cell-free supernatants after 24 h of LPS challenge and normalized with the number of cells. The bars (mean + SEM) are normalized values as percent of measured levels of CXCL1/KC in cell-free supernatants of LPS-challenged cells. The results are derived from three-six experiments performed on separate occasions, and the *t*-test was used for statistical analysis.

present in the biological system and tissue microenvironment. For an example, change in the conformation of 37-residue human antibacterial peptide LL-37 at acidic pH diminishes its activity. Specifically, helical content of LL-37 decreases at pH < 5.0, and the conformation is completely disordered at a pH < 2.0.[37] In another instance, the antibacterial activity of hepcidin 20 and 25 is increased at acidic pH 5.0 and 6.6.[38] While the structure and physicochemical properties of SPA4 peptide are compatible for binding to TLR4 and anti-inflammatory activity,[27,33] the stability and structure–activity relation of SPA4 peptide remained unknown under ambient and stressed conditions.

The results of this study demonstrate the stability of the structure of the SPA4 peptide at room temperature and at 4 °C during a study period of 10 days (Fig. 2). These results are consistent with its stability in prescribed storage in frozen state over its shelf-life of 6 months.[5] The primary structure of the SPA4 peptide also is not affected when maintained at physiological concentration of 100 μM in phosphate buffer solutions of pH 5.7, 7.0, and 8.0 for 1 h at temperatures of 25–37 °C. However, the peptide bonds of SPA4 peptide are disrupted and absorbance peaks are shifted at pH 3.0 and 10.0 (Fig. 3).

Simulated lung fluids (Gamble's solution and ALF) were included to evaluate the stability of the primary structure of the SPA4 peptide in the presence of different electrolytes and salts as observed in healthy and injured lungs. However, the organic acids, proteins, and lung surfactant were not incorporated in these solutions.[21] Research studies in the past have used Gamble's solution and ALF mainly to determine dissolution, solubility, and physical properties of inhaled materials and nanoparticles.[39–41] The original UV-VIS spectra of the SPA4 peptide in both fluids were comparable to that in water (Fig. 4), but peak shifts were identified between wavelengths 240–310 nm. The original UV-VIS spectra remained unaltered in all the chemical components of simulated lung fluids except for sodium hydroxide, one of the components of ALF (Table 2). Also, slightly lower absorbance values were obtained for SPA4 peptide in magnesium chloride, sodium lactate, sodium pyruvate, and sodium tartrate dihydrate solutions. Alterations were identified in the form of shifts in peaks, derivative values, and vibrational fine structures within fourth-derivate UV-VIS spectra of SPA4 peptide incubated in distinct chemical solutions at prescribed concentrations in simulated lung fluids.

The physiological concentrations of all these chemical components of simulated lung fluids are not completely known in healthy or injured lungs. However, one of the hallmarks of acute lung inflammation and injury is the alteration of electrolyte levels. Hyponatremia, hypomagnesemia, and hypokalemia are commonly observed in various lung diseases[42–51] Citrate produced during tricarboxylic acid cycle or Kreb's cycle of cellular respiration activates immune cells and production of proinflammatory mediators.[52] Accumulation of citrate also results into death of alveolar epithelial cells during LPS-induced injury due to necroptosis.[53] Dysregulated glycolysis and metabolic pathways are associated with an inflammatory response during tissue injuries.[54] An elevated level of lactate is frequently observed in critically ill patients, and is prognostic marker of mortality in patients with ARDS.[25,26] And, reduced lactate in serum is associated with higher survival among patients with acute respiratory failure.[55–57] Our results show the LPS-stimulated CXCL1/KC and lactate secretion by mouse lung epithelial cells (Fig. 9), which corroborates with an increased accumulation of lactate in serum and lung tissue homogenates of the mouse models of lung infection and inflammation.[3,58] Therapeutic treatment with the SPA4 peptide reduces the secreted levels of lactate and CXCL1/KC in mouse models[3,58] and in lung epithelial cells (Fig. 9). Since the SPA4 peptide is given therapeutically, we questioned whether the structure–activity relationship of the SPA4 peptide is affected in presence of lactate.

The original and fourth-derivative UV-VIS spectra of the SPA4 peptide in 2 mM sodium lactate solution overlapped with those in water after 24 h incubation at room temperature (Fig. 10A). And secondary structure was maintained for SPA4 peptide in 2 mM sodium lactate solution as evident by CD spectrum in Fig. 10C. The characteristics of secondary structure of SPA4 peptide (Fig. 10C) were similar to those of SPA4 peptide in water as published earlier.[5,27,33] As published earlier, the UV-VIS spectrum of SPA4 peptide depicts the absorbance peaks at wavelength range of 200–220 nm due to its backbone peptide bonds.[27] However, lower absorbance readings and a slight shift

in peaks were noted for SPA4 peptide maintained in 500 mM sodium lactate solution indicating affected backbone peptide bonds (Fig. 10B).

An assessment of activity included the SPA4 peptide with intact or disrupted structure after pre-incubation in water (vehicle), 2 mM sodium lactate or 500 mM sodium lactate for 24 h at room temperature. The SPA4 peptide was diluted to 100 μM for cell treatments against LPS challenge (Fig. 11). As per Fig. 9, the secreted levels of CXCL/KC were considered as an end-point study parameter for SPA4 peptide activity against LPS stimuli. Our results demonstrated suppression of LPS-induced secretion of CXCL1/KC by SPA4 peptide with intact structure after pre-incubation in water or 2 mM sodium lactate (Fig. 11). Together, these results reveal the stability and structure–activity relationship of the SPA4 peptide in ambient conditions and simulated fluids and systems mimicking lung injury. Further studies are warranted to delineate the molecular mechanism of cellular metabolism during injury and the effect of SPA4 peptide on lung homeostasis.

Author contributions

AAC performed the experiments and assays, collected, and analyzed data, and wrote the original draft of the manuscript. KR determined the secondary structure by CD spectroscopy. NMG assisted with determination of CXCL1/KC levels by ELISA. SA designed and coordinated the study and helped with lung epithelial cell isolation, data analysis, and organization and compilation of the manuscript. Research reported here was supported by a grant award from the National Heart, Lung, and Blood Institute of the National Institute of Health (award number R01 HL136325). The content is solely the responsibility of the authors and does not necessarily represent the official views of the National Institute of Health.

Additional disclosures

Part of the work was presented at the American Thoracic Society 2023 International Conference, May 19–24, 2023, Washington DC, USA. Published version of this manuscript will be included in entirety within AAC's Ph.D. dissertation thesis after approval from the Journal's office of publication. The Ph.D. thesis dissertation will be made available in public domain after publication of the manuscript.

Conflicts of interest

There are no conflicts of interest to declare.

Acknowledgements

Authors thank Dr Mary Carter, Writing Center at OUHSC, Oklahoma City, OK, for providing editorial assistance.

References

1 K. A. Fitzgerald, D. C. Rowe and D. T. Golenbock, Endotoxin recognition and signal transduction by the TLR4/MD2-complex, *Microbes Infect.*, 2004, **6**(15), 1361–1367.
2 S. Awasthi, K. Brown, C. King, V. Awasthi and R. Bondugula, A toll-like receptor-4-interacting surfactant protein-A-derived peptide suppresses tumor necrosis factor-α release from mouse JAWS II dendritic cells, *J. Pharmacol. Exp. Ther.*, 2011, **336**(3), 672–681.
3 S. Awasthi, B. Singh, V. Ramani, J. Xie and S. Kosanke, TLR4-interacting SPA4 peptide improves host defense and alleviates tissue injury in a mouse model of *Pseudomonas aeruginosa* lung infection, *PLoS One*, 2019, **14**(1), e0210979.
4 V. Ramani, R. Madhusoodhanan, S. Kosanke and S. Awasthi, A TLR4-interacting SPA4 peptide inhibits LPS-induced lung inflammation, *Innate Immun.*, 2013, **19**(6), 596–610.
5 A. A. Chowdhury, N. M. Godbole, N. Chataut, S. Kosanke, K. Rodgers and S. Awasthi, Effects of SPA4 peptide on lipopolysaccharide-disrupted lung epithelial barrier, injury, and function in a human cell system and mouse model of lung injury, *Physiol. Rep.*, 2022, **10**(13), e15353.
6 H. Fischer and J. H. Widdicombe, Mechanisms of acid and base secretion by the airway epithelium, *J. Membr. Biol.*, 2006, **211**(3), 139–150.
7 M. Zajac, E. Dreano, A. Edwards, G. Planelles and I. Sermet-Gaudelus, Airway surface liquid pH regulation in airway epithelium current understandings and gaps in knowledge, *Int. J. Mol. Sci.*, 2021, **22**(7), 3384.
8 C. R. Bodem, L. M. Lampton, D. P. Miller, E. F. Tarka and E. D. Everett, Endobronchial pH. Relevance of aminoglycoside activity in gram-negative bacillary pneumonia, *Am. Rev. Respir. Dis.*, 1983, **127**(1), 39–41.
9 S. Tate, G. MacGregor, M. Davis, J. A. Innes and A. P. Greening, Airways in cystic fibrosis are acidified: detection by exhaled breath condensate, *Thorax*, 2002, **57**(11), 926–929.
10 X. X. Tang, L. S. Ostedgaard, M. J. Hoegger, T. O. Moninger, P. H. Karp, J. D. McMenimen, B. Choudhury, A. Varki, D. A. Stoltz and M. J. Welsh, Acidic pH increases airway surface liquid viscosity in cystic fibrosis, *J. Clin. Invest.*, 2016, **126**(3), 879–891.
11 J. F. Hunt, K. Fang, R. Malik, A. Snyder, N. Malhotra, T. A. Platts-Mills and B. Gaston, Endogenous airway acidification. Implications for asthma pathophysiology, *Am. J. Respir. Crit. Care Med.*, 2000, **161**(3 Pt 1), 694–699.
12 E. Lozo Vukovac, K. Miše, I. Gudelj, I. Perić, D. Duplančić, I. Vuković, Z. Vučinović and M. Lozo, Bronchoalveolar pH and inflammatory biomarkers in patients with acute exacerbation of chronic obstructive pulmonary disease, *J. Int. Med. Res.*, 2019, **47**(2), 791–802.
13 K. Kostikas, G. Papatheodorou, K. Ganas, K. Psathakis, P. Panagou and S. Loukides, pH in expired breath condensate of patients with inflammatory airway diseases, *Am. J. Respir. Crit. Care Med.*, 2002, **165**(10), 1364–1370.

14 H. Fischer, J. H. Widdicombe and B. Illek, Acid secretion and proton conductance in human airway epithelium, *Am. J. Physiol.: Cell Physiol.*, 2002, **282**(4), C736–C743.
15 A. S. Trevani, G. Andonegui, M. Giordano, D. H. López, R. Gamberale, F. Minucci and J. R. Geffner, Extracellular acidification induces human neutrophil activation, *J. Immunol.*, 1999, **162**(8), 4849–4857.
16 S. Metwaly, A. Cote, S. J. Donnelly, M. M. Banoei, A. I. Mourad and B. W. Winston, Evolution of ARDS biomarkers: Will metabolomics be the answer?, *Am. J. Physiol.: Lung Cell. Mol. Physiol.*, 2018, **315**(4), L526–L534.
17 W. Roque and F. Romero, Cellular metabolomics of pulmonary fibrosis, from amino acids to lipids, *Am. J. Physiol.: Cell Physiol.*, 2021, **320**(5), C689–C695.
18 W. Cheng, K. E. Duncan, A. J. Ghio, C. Ward-Caviness, E. D. Karoly, D. Diaz-Sanchez, R. B. Conolly and R. B. Devlin, Changes in metabolites present in lung-lining fluid following exposure of humans to ozone, *Toxicol. Sci.*, 2018, **163**(2), 430–439.
19 J. Z. Hu, D. N. Rommereim, K. R. Minard, A. Woodstock, B. J. Harrer, R. A. Wind, R. P. Phipps and P. J. Sime, Metabolomics in lung inflammation:a high-resolution (1)h NMR study of mice exposed to silica dust, *Toxicol. Mech. Methods*, 2008, **18**(5), 385–398.
20 C. Manni, S. I. Magalini and A. F. Sabato, Biochemical changes in acute respiratory failure, *Resuscitation*, 1981, **9**(4), 275–281.
21 E. Innes, H. H. P. Yiu, P. McLean, W. Brown and M. Boyles, Simulated biological fluids - a systematic review of their biological relevance and use in relation to inhalation toxicology of particles and fibres, *Crit. Rev. Toxicol.*, 2021, **51**(3), 217–248.
22 E. E. Douzinas, P. D. Tsidemiadou, M. T. Pitaridis, I. Andrianakis, A. Bobota-Chloraki, K. Katsouyanni, D. Sfyras, K. Malagari and C. Roussos, The regional production of cytokines and lactate in sepsis-related multiple organ failure, *Am. J. Respir. Crit. Care Med.*, 1997, **155**(1), 53–59.
23 S. D. Brown, C. Clark and G. Gutierrez, Pulmonary lactate release in patients with sepsis and the adult respiratory distress syndrome, *J. Crit. Care*, 1996, **11**(1), 2–8.
24 D. De Backer, J. Creteur, H. Zhang, M. Norrenberg and J. L. Vincent, Lactate production by the lungs in acute lung injury, *Am. J. Respir. Crit. Care Med.*, 1997, **156**(1), 1099–1104.
25 J. A. Kellum, D. J. Kramer, K. Lee, S. Mankad, R. Bellomo and M. R. Pinsky, Release of lactate by the lung in acute lung injury, *Chest*, 1997, **111**(5), 1301–1305.
26 T. Kamo, S. Tasaka, T. Suzuki, T. Asakura, S. Suzuki, K. Yagi, H. Namkoong, M. Ishii, H. Morisaki and T. Betsuyaku, Prognostic values of the Berlin definition criteria, blood lactate level, and fibroproliferative changes on high-resolution computed tomography in ARDS patients, *BMC Pulm. Med.*, 2019, **19**(1), 37.
27 S. Awasthi, G. Kumar, V. Ramani, V. Awasthi, K. K. Rodgers, J. Xie, J. Beierle, G. Kyere-Davies, B. Singh, N. Rahman, A. A. Chowdhury and N. Chataut, Mechanism of anti-inflammatory activity of TLR4-interacting SPA4 peptide, *Immunohorizons*, 2021, **5**(8), 659–674.
28 A. Savitzky and J. E. Golay, Smoothing and differentiation of data by simplified least squares procedures, *Anal. Chem.*, 1964, **36**(8), 1627–1639.
29 M. R. Liyanage, K. Bakshi, D. B. Volkin and C. R. Middaugh, Ultraviolet absorption spectroscopy of peptides, *Methods Mol. Biol.*, 2014, **1088**, 225–236.
30 V. S. Stoll and J. S. Blanchard, Buffers: principles and practice, *Methods Enzymol.*, 1990, **182**, 24–38.
31 G. Gomori, Preparation of buffers for use in enzyme studies, *Methods Enzymol.*, 1955, **1**, 138–146.
32 A. Kanavarioti, C. F. Bernasconi, D. L. Doodokyan and D. J. Alberas, Magnesium ion catalyzed P-N bond hydrolysis in imidazolide-activated nucleotides. Relevance to template-directed synthesis of polynucleotides, *J. Am. Chem. Soc.*, 1989, **111**(18), 7247–7257.
33 S. Awasthi, A. Anbanandam and K. K. Rodgers, Structure of a TLR4-interacting SPA4 peptide, *RSC Adv.*, 2015, **5**(35), 27431–27438.
34 L. J. Godderz, N. S. Rahman, G. M. Risinger, J. L. Arbuckle and K. K. Rodgers, Self-association and conformational properties of RAG1: implications for formation of the V(D)J recombinase, *Nucleic Acids Res.*, 2003, **31**(7), 2014–2023.
35 M. Sinha and C. A. Lowell, Isolation of highly pure primary mouse alveolar epithelial type II cells by flow cytometric cell sorting, *Bio-Protoc.*, 2016, **6**(22), e2013.
36 R. M. Viscardi, S. Ullsperger and J. H. Resau, Reproducible isolation of type II pneumocytes from fetal and adult rat lung using nycodenz density gradients, *Exp. Lung Res.*, 1992, **18**(2), 225–245.
37 J. Johansson, G. H. Gudmundsson, M. E. Rottenberg, K. D. Berndt and B. Agerberth, Conformation-dependent antibacterial activity of the naturally occurring human peptide LL-37, *J. Biol. Chem.*, 1998, **273**(6), 3718–3724.
38 G. Maisetta, R. Petruzzelli, F. L. Brancatisano, S. Esin, A. Vitali, M. Campa and G. Batoni, Antimicrobial activity of human hepcidin 20 and 25 against clinically relevant bacterial strains: effect of copper and acidic pH, *Peptides*, 2010, **31**(11), 1995–2002.
39 L. Zhong, X. Liu, X. Hu, Y. Chen, H. Wang and H. Z. Lian, *In vitro* inhalation bioaccessibility procedures for lead in PM(2.5) size fraction of soil assessed and optimized by *in vivo–in vitro* correlation, *J. Hazard. Mater.*, 2020, **381**, 121202.
40 R. F. Hamilton, Z. Wu, M. Thakkar, A. Holian and S. Mitra, Modification of nano-silver bioactivity by adsorption on carbon nanotubes and graphene oxide, *Inhalation Toxicol.*, 2018, **30**(11–12), 429–438.
41 S. Latvala, J. Hedberg, S. Di Bucchianico, L. Moller, I. Odnevall Wallinder, K. Elihn and H. L. Karlsson, Nickel release, ROS generation and toxicity of Ni and NiO micro- and nanoparticles, *PLoS One*, 2016, **11**(7), e0159684.
42 M. Cuesta, D. Slattery, E. L. Goulden, S. Gupta, E. Tatro, M. Sherlock, W. Tormey, S. O'Neill and C. J. Thompson, Hyponatraemia in patients with community-acquired pneumonia; prevalence and aetiology, and natural history of SIAD, *Clin. Endocrinol.*, 2019, **90**(5), 744–752.

43 M. T. García-Sanz, S. Martínez-Gestoso, U. Calvo-Álvarez, L. Doval-Oubiña, S. Camba-Matos, C. Rábade-Castedo, C. Rodríguez-García and F. J. González-Barcala, Impact of hyponatremia on COPD exacerbation prognosis, *J. Clin. Med.*, 2020, **9**(2), 503.

44 I. Fiordoliva, T. Meletani, M. G. Baleani, S. Rinaldi, A. Savini, M. Di Pietro Paolo and R. Berardi, Managing hyponatremia in lung cancer: latest evidence and clinical implications, *Ther. Adv. Med. Oncol.*, 2017, **9**(11), 711–719.

45 R. Padhi, B. N. Panda, S. Jagati and S. C. Patra, Hyponatremia in critically ill patients, *Indian J. Crit. Care Med.*, 2014, **18**(2), 83–87.

46 G. Faa, L. Saba, D. Fanni, G. Kalcev and M. Carta, Association between hypomagnesemia, COVID-19, respiratory tract and lung disease, *Open Respir. Med. J.*, 2021, **15**, 43–45.

47 H. Kılıc, A. Kanbay, A. Karalezlı, E. Babaoglu, H. C. Hasanoglu, O. Erel and C. Ates, The relationship between hypomagnesemia and pulmonary function tests in patients with chronic asthma, *Med. Princ. Pract.*, 2018, **27**(2), 139–144.

48 S. Makwana, A. Patel and M. Sonagara, Correlation between serum magnesium level and acute exacerbation in patients with chronic obstructive pulmonary disease (COPD), *Cureus*, 2022, **14**(6), e26229.

49 O. Moreno-Pérez, J.-M. Leon-Ramirez, L. Fuertes-Kenneally, M. Perdiguero, M. Andres, M. Garcia-Navarro, P. Ruiz-Torregrosa, V. Boix, J. Gil, E. Merino, S. Asensio, C. Fernandez, A. Candela, M. del Mar García, R. Sánchez, S. Reus, P. Ruiz, R. García-Sevila, M.-Á. Martínez, M.-M. García-Mullor, M. Blanes, J. Guijarro, J. C. Pascual, I. Gonzalez, P. Sanso, J. M. Ramos, J. Javaloy, C. Llopis, O. Coronado, E. García, G. Rodríguez, P. Melgar, M. Franco, F. Lluís, C. Zaragoza, C. Alcaraz, A. Carrión, C. Villodre, E. R. de la Cuesta, C. Alenda, F. Peiró, M. Planelles, L. Greco, S. Silvia, A. Francia, I. Verdú, J. Sales, A. Palacios, H. Ballester, A. García-Valentín, M. Márquez, E. Canelo, A. Juan and E. Vives, Hypokalemia as a sensitive biomarker of disease severity and the requirement for invasive mechanical ventilation requirement in COVID-19 pneumonia: A case series of 306 Mediterranean patients, *Int. J. Infect. Dis.*, 2020, **100**, 449–454.

50 S. Ravioli, R. Gygli, G. C. Funk, A. Exadaktylos and G. Lindner, Prevalence and impact on outcome of sodium and potassium disorders in patients with community-acquired pneumonia: A retrospective analysis, *Eur. J. Intern. Med.*, 2021, **85**, 63–67.

51 G. Lindner, S. Herschmann, G. C. Funk, A. K. Exadaktylos, R. Gygli and S. Ravioli, Sodium and potassium disorders in patients with COPD exacerbation presenting to the emergency department, *BMC Emerg. Med.*, 2022, **22**(1), 49.

52 N. C. Williams and L. A. J. O'Neill, A role for the Krebs cycle intermediate citrate in metabolic reprogramming in innate immunity and inflammation, *Front. Immunol.*, 2018, **9**, 141.

53 H. H. Yang, H. L. Jiang, J. H. Tao, C. Y. Zhang, J. B. Xiong, J. T. Yang, Y. B. Liu, W. J. Zhong, X. X. Guan, J. X. Duan, Y. F. Zhang, S. K. Liu, J. X. Jiang, Y. Zhou and C. X. Guan, Mitochondrial citrate accumulation drives alveolar epithelial cell necroptosis in lipopolysaccharide-induced acute lung injury, *Exp. Mol. Med.*, 2022, **54**(11), 2077–2091.

54 G. Soto-Heredero, M. M. Gomez de Las Heras, E. Gabande-Rodriguez, J. Oller and M. Mittelbrunn, Glycolysis - a key player in the inflammatory response, *FEBS J.*, 2020, **287**(16), 3350–3369.

55 Y. F. Zhao, Y. Lin and X. L. Zhu, [Clinical significance of early lactate clearance rate in patients with respiratory failure], *Zhonghua Jiehe He Huxi Zazhi*, 2010, **33**(3), 183–187.

56 Z. Zang, H. Xu, L. Dong, F. Gao and J. Yan, [Prognostic significance of early lactate clearance rate for severe acute respiratory failure patients on extracorporeal membrane oxygenation], *Zhonghua Jiehe He Huxi Zazhi*, 2014, **37**(3), 197–201.

57 W. H. Wu, Y. Y. Niu, C. R. Zhang, L. B. Xiao, H. S. Ye, D. M. Pan and M. Zeng, Combined APACH II score and arterial blood lactate clearance rate to predict the prognosis of ARDS patients, *Asian Pac. J. Trop. Med.*, 2012, **5**(8), 656–660.

58 S. Awasthi, N. Rahman, B. Rui, G. Kumar, V. Awasthi, M. Breshears and S. Kosanke, Lung and general health effects of Toll-like receptor-4 (TLR4)-interacting SPA4 peptide, *BMC Pulm. Med.*, 2020, **20**(1), 179.